JACS
JOURNAL OF THE AMERICAN CHEMICAL SOCIETY
pubs.acs.org/JACS
Article

Atomic-Scale Visualization of Heterolytic H_2 Dissociation and CO_x Hydrogenation on ZnO under Ambient Conditions

Yunjian Ling,[○] Jie Luo,[○] Yihua Ran, Zhi Liu, Wei-Xue Li,* and Fan Yang*

Cite This: *J. Am. Chem. Soc.* 2023, 145, 22697−22707
Read Online

ABSTRACT: Studying catalytic hydrogenation reactions on oxide surfaces at the atomic scale has been challenging because of the typical occurrence of these processes at ambient or elevated pressures, rendering them less accessible to atomic-scale techniques. Here, we report an atomic-scale study on H_2 dissociation and the hydrogenation of CO and CO_2 on ZnO using ambient pressure scanning tunneling microscopy, ambient pressure X-ray photoelectron spectroscopy, and density functional theory (DFT) calculations. We directly visualized the heterolytic dissociation of H_2 on ZnO($10\bar{1}0$) under ambient pressure and found that dissociation reaction does not require the assistance of surface defects. The presence of CO or CO_2 on ZnO at 300 K does not impede the availability of surface sites for H_2 dissociation; instead, CO can even enhance the stability of coadsorbed hydride species, thereby facilitating their dissociative adsorption. Our results show that hydride is the active species for hydrogenation, while hydroxyl cannot hydrogenate CO/CO_2 on ZnO. Both AP studies and DFT calculations showed that the hydrogenation of CO_2 on ZnO is thermodynamically and kinetically more favorable compared to that of CO hydrogenation. Our results point toward a two-step mechanism for CO hydrogenation, involving initial oxidation to CO_2 at step sites on ZnO followed by reaction with hydride to form formate. These findings provide molecular insights into the hydrogenation of CO/CO_2 on ZnO and deepen our understanding of syngas conversion and oxide catalysis in general.

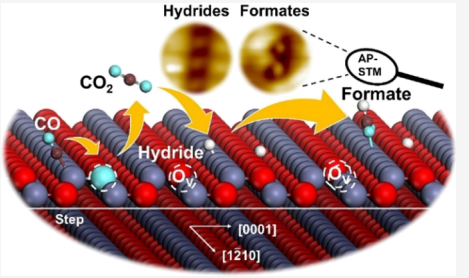

1. INTRODUCTION

The catalytic hydrogenation of CO and CO_2 into valuable chemicals,[1] utilizing eco-friendly hydrogen from renewable resources, holds high importance in carbon capture and utilization (CCU) and facilitating the clean utilization of coal, natural gas, and biomass. Oxide catalysts for hydrogenation reactions[2−4] have increasingly caught attention due to their high selectivity. In this regard, ZnO is particularly crucial for the catalytic hydrogenation of CO[4,5] and CO_2.[6,7] ZnO-based oxides, when integrated into bifunctional oxide-zeolite (OXZEO) composite catalysts, demonstrated a most promising catalytic performance for syngas conversion.[3,4,8] ZnO-supported metal nanoparticles are also widely employed as major catalysts for methanol synthesis[9] and the reverse water gas shift reaction (RWGS).[10,11] As such, research interest in the role of ZnO in catalytic hydrogenation reactions has surged, making it a central focus within the catalysis field in recent years. Although industrial catalysts typically used the combination with supported metal catalysts or zeolites, the importance of ZnO in H_2 dissociation and H spillover has been highlighted by Mehar et al.[12] on hydrogenation reactions at the ZnO-Cu interface. ZnO powders alone have also been employed in reaction mechanism studies of CO_x hydrogenation, which could also lead to the formation of methanol[13] or methane,[14] depending on reaction conditions.

Hydrogen adsorption and dissociation on metal oxides are central to diverse applications, including hydrogen sensing[15] and hydrogenation catalysis.[8,16−18] Two primary mechanisms underpin H_2 dissociation on oxide surfaces: homolytic and heterolytic cleavage. Homolytic cleavage leads to the formation of two hydrogen atoms at oxygen sites, resulting in the generation of OH groups and the simultaneous reduction of surface metal ions. This process is particularly favorable on oxides, such as TiO_2[19] and CeO_2,[20] that exhibit high reducibility. On the other hand, heterolytic cleavage involves the formation of hydride (H^-) and proton (H^+) species at metal and oxygen sites, respectively, yielding M−H and OH entities. Heterolytic cleavage is favored on oxides, such as MgO[21] and Al_2O_3,[22] that are difficult to reduce, although certain reducible oxides, including Ga_2O_3,[23] Cr_2O_3,[24] and ZnO,[25] have been reported to exhibit this mechanism in the presence of defects. Heterolytic dissociation of H_2 has been proposed for H_2 adsorption on ZnO, leading to the formation of hydride and hydroxyl species.[26] However, the exact active site structure responsible for the heterolytic dissociation on ZnO, whether it involves defects or not, remains unclear.

Received: July 27, 2023
Published: October 6, 2023

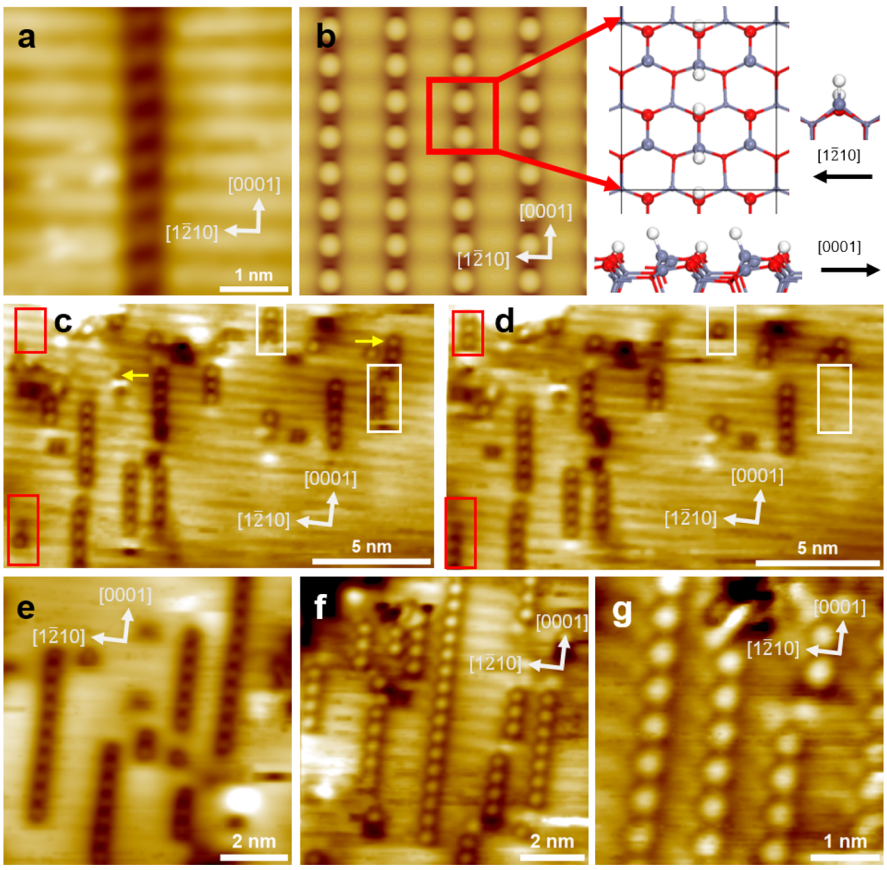

Figure 1. (a) Atomically resolved and (b) simulated STM images of hydride species on ZnO($10\bar{1}0$) in 0.4 mbar H_2 at 300 K. The corresponding structural model of hydride chains is displayed in panel (b). Gray, red, and white spheres represent Zn, lattice O, and H atoms, respectively. (c, d) In situ STM images of hydride species on ZnO($10\bar{1}0$) in 0.4 mbar of H_2 at 300 K. Red and white rectangles mark the formation and disappearance of surface hydride species via the dissociative adsorption and recombinative desorption of H_2, respectively. Yellow arrows indicate the diffusion of surface hydride species. (e–g) STM images of hydride species on ZnO($10\bar{1}0$) in 2 mbar H_2/CO (3:1) mixture gas at 300 K. Scanning parameters: (a) V_s = 2.4 V, I_t = 130 pA, (c) V_s = 2.4 V, I_t = 160 pA, (d) V_s = 2.4 V, I_t = 130 pA, and (e–g) V_s = 2.4 V, I_t = 110 pA.

In hydrogenation reactions, hydroxyl groups are relatively stable during the reaction and have been extensively studied. Recently, the formation of surface and bulk hydride species upon the heterolytic dissociation of H_2 has been demonstrated using inelastic neutron spectroscopy studies[27] and proposed as important intermediates for hydrogenation catalysis. However, the role of hydride species has been less discussed due to their low concentrations and challenges in isolating their effects from the abundance of hydroxyl groups on oxide powders. So far, mechanistic studies of hydrogenation catalysis on oxides are almost exclusively performed on powder catalysts,[28] which limited the accurate identification of key intermediates/reaction path due to their complex surface composition and morphology. In contrast to metal surfaces, there is a lack of mechanistic studies of well-defined metal oxide surfaces regarding hydrogenation reactions of small molecules. The specific adsorption sites and detailed reaction properties of these systems are mostly unknown. One significant challenge is that active hydrogen species tend to desorb under vacuum conditions, while hydrogenation reactions typically necessitate higher pressures, as evidenced by powder catalysis. This dichotomy has made vacuum-based surface science approaches, including molecular beam studies,[29] difficult for detecting hydrogenated intermediates/products. Ambient pressure scanning tunneling microscopy (AP-STM) provides an apt tool for atomic-scale studies of hydrogenation catalysis and trace hydroxyl or hydride species on well-defined model catalysts. Its usage has been limited, partly due to the challenge of maintaining a stable tunneling junction on bulk oxide surfaces in a reactive environment.

In this study, we used a combination of ambient pressure scanning tunneling microscopy (AP-STM), ambient pressure X-ray photoelectron spectroscopy (AP-XPS), and density functional theory (DFT) calculations to understand the hydrogenation of CO and CO_2 on ZnO($10\bar{1}0$) at the atomic and molecular level. ZnO($10\bar{1}0$), as the most stable facet of ZnO,[30] has been most studied among model ZnO surfaces. Li et al.[31] has also observed an enhanced hydrogenation activity on the ZnO($10\bar{1}0$) facet in syngas conversion. The preeminence of ZnO($10\bar{1}0$) during catalytic reactions underscores the necessity to comprehend its surface structure and chemical and reaction properties. Previous studies[32,33] have suggested that weakly adsorbed species could play a significant role in hydrogenation catalysis, but in situ experimental studies have been limited owing to the difficulties to probe physisorbed species under ambient conditions. Here, our use of AP-STM has allowed the direct visualization of H_2 dissociation and hydrogenation reactions on ZnO under ambient pressures at the atomic level. The heterolytic dissociation of H_2 was found to occur on the planar terrace of ZnO, while hydride species are free to diffuse across the surface. By controlling the formation of hydride or hydroxyl species on the ZnO surface, we were able to study the reaction between CO/CO_2 and the surface hydride or hydroxyl

https://doi.org/10.1021/jacs.3c08085
J. Am. Chem. Soc. 2023, 145, 22697−22707

species separately. Our results showed that although hydride and hydroxyl species are formed together during the dissociative adsorption of H_2, they have opposite effects on the subsequent reaction with CO/CO_2. This allowed us to identify the catalytic roles of these surface species and to understand the mechanisms of CO and CO_2 hydrogenation on ZnO.

2. EXPERIMENTAL SECTION

AP-STM studies were performed in a customized STM system, which contains an AP-STM (SPECS, base pressure $<3 \times 10^{-10}$ mbar) with a near-ambient pressure (NAP) cell,[34] which enables the sample to be heated up to 500 K under AP conditions. AP-XPS studies were performed in a customized lab-based AP-XPS instrument (SPECS, base pressure $<8 \times 10^{-10}$ mbar),[35] which contains a NAP hemispherical electron energy analyzer (PHOIBOS) and a microfocus monochromatized Al Kα X-ray source.

ZnO$(10\bar{1}0)$ (MatecK) was treated by two to three cycles of Ar^+ sputtering (1 keV, 10 μA) and annealing (1100 K) for impurity removement. The final annealing step should be operated at 900 K with subsequent annealing at 650 K in the presence of 3×10^{-8} mbar of H_2 for avoiding surface defects and maintaining the conductivity of ZnO$(10\bar{1}0)$. The H_2/CO and H_2/CO_2 mixtures were obtained by mixing pure H_2, CO, and CO_2 (Arkonic) in a gas mixing chamber and then were introduced to the NAP cell. For in situ AP-STM experiments at elevated temperatures, high-resolution STM images were typically acquired during cooling to near 300 K to avoid severe drifts. STM images were obtained by using Pt/Ir tips and processed with SPIP (Image Metrology).

Fourier-transformed infrared spectroscopy (FTIR) measurements were performed in a homemade ultrahigh vacuum (UHV) in situ IR cell, and its details have been mentioned in a previous study.[36] ZnO rods used in FTIR measurements were prepared by the method described in a previous study.[5] IR spectra were recorded with 128 scans at a 4 cm^{-1} resolution.

Density functional theory (DFT) calculations were performed by the Vienna ab initio simulation package (VASP) using PAW potential,[37−39] the exchange−correlation interaction was described via the optB86b-vdW functional,[40] and the electronic analysis was calculated by the Perdew−Burke−Ernzerhof (PBE) exchange-correlation functional.[41] As shown previously,[42,43] the method used (DFT, DFT + U) has little influence on the description of binding energy and reaction barriers. The plane wave basis set with a kinetic energy cutoff of 400 eV was used to solve the Kohn−Sham equations. The optimized lattice constants of bulk wurtzite ZnO are $a = b = 3.29$ Å with $c = 5.30$ Å, which are consistent with the experimental results ($a = b = 3.25$ Å with $c = 5.21$ Å).[44,45] ZnO$(10\bar{1}0)$ surfaces were modeled by a three double-layer slab model separated by 12 Å vacuum along the Z direction. The $(2 \times 2 \times 1)$ and $(3 \times 2 \times 1)$ k-point meshes were used to sample the Brillouin zone for (3×2) and (2×2) periodicity slab models. The bottom-one layer of the slab was fixed, and the remaining atoms were relaxed until the residual forces were less than 0.02 eV/Å. The climbing image nudged elastic band (CI-NEB) method[46,47] was carried out to identify the transition states and then verified to possess only one vibrational mode with a negative curvature in the direction of bond breaking or forming process. The STM images were simulated on the basis of Tersoff and Hamann's formula[48−50] using the bSKAN code.[51−53]

3. RESULTS AND DISCUSSION

3.1. H_2 Dissociation and Hydride Formation on ZnO$(10\bar{1}0)$. The formation of hydride species on ZnO requires the exposure of the material to ambient pressure H_2. In UHV, the interaction between H_2 and ZnO is weak, and no adsorption or reaction of H_2 was observed on ZnO at above 80 K. However, when ZnO was exposed to 13 mbar H_2 at 154 K, our FTIR measurements (Figure S1) show the emergence of two peaks at 3495 and 1707 cm^{-1}, corresponding to the stretch vibration peaks of O−H and Zn−H,[26] respectively. We thus used AP-STM to study the formation of hydride species on ZnO$(10\bar{1}0)$ (Figure S2) at the atomic level. When ZnO$(10\bar{1}0)$ was exposed to 0.4 mbar of H_2 at 300 K, Figure 1a shows the formation of hydrogen chains along the [0001] direction of the surface. These chains consist of bright dots located on the Zn sites (Figure S3a). STM simulations (Figure 1b) suggest that these dots correspond to the hydride species formed from the heterolytic dissociation of H_2 as both the projected density of states (PDOS) and the geometric locations of H atoms on Zn sites are higher than those of H atoms on the O sites (Figure S4). The neighboring O−H species appear as depressions in the STM simulation and are not visible in STM images. Similar features could be observed on ZnO$(10\bar{1}0)$ when the surface is exposed to H_2 at 20 K.[54] Thus, H_2 dissociation on ZnO$(10\bar{1}0)$ is likely a barrierless process and prefers to occur on the planar terrace of ZnO, without the assistance of surface defects. The formation of hydride chains also suggests that heterolytically dissociated hydrogen pairs tend to undergo dissociative adsorption at neighboring sites, similar to the dissociative adsorption of O_2 on Pt at cryogenic temperatures.[55]

During the gradual increase in H_2 pressure to 0.4 mbar on ZnO$(10\bar{1}0)$, the surface coverage of hydride chains gradually reached ~0.01 ML (Figure S3a). However, when the H_2 pressure was further raised to 1 bar, the increase in surface hydride chains was less noticeable (Figure S3b). This suggests that surface hydride species on ZnO$(10\bar{1}0)$ is in dynamic equilibrium with gas-phase H_2 at 300 K, and surface Zn sites are far from being saturated. In situ STM measurements (Figure 1c,d) also observed the fluctuation and diffusion of hydride chains, which indicates the recombinative desorption and dissociative adsorption of H_2 on ZnO$(10\bar{1}0)$. When surface hydrides desorbed, no defects were observed on the surface, suggesting that surface hydrides prefer to recombine with neighboring hydrogen on lattice oxygen to form H_2, which then leaves the surface. These observations are consistent with DFT calculation results[56] and the temperature-programmed desorption study.[57] In dynamic equilibrium, the diffusion of surface hydrides on ZnO$(10\bar{1}0)$ preferentially occurred along the $[1\bar{2}10]$ direction of the Zn row, as indicated in Figure 1c. The coadsorption of CO has an effect in enhancing the atomic resolution of AP-STM, where hydride atoms turned into bright balls (Figure 1e−g). The enhanced image contrast induced by CO adsorption at the tip apex has been recognized and practiced in low-temperature STM and qplus AFM studies, and in our case, we found that such a principle is also applicable to AP-STM studies.

DFT calculations show that the dissociative adsorption energy of the first H_2 molecule on ZnO$(10\bar{1}0)$ is −0.48 eV (Figure S5a). The second H_2 molecule has an adsorption energy of −0.76 eV when adsorbed in the [0001] direction (Figure S5b) but −0.26 eV when adsorbed in the $[1\bar{2}10]$ direction (Figure S5c). The differences in adsorption energies indicate that there is an attractive interaction between neighboring H atoms along the [0001] direction and a repulsion between neighboring H atoms along the $[1\bar{2}10]$ direction. Bader charge analysis also shows that the hydride species on Zn sites have a negative Bader charge of −0.40 |e|, while H atoms bonded to O sites have a positive Bader charge of +0.27 |e|. In the H chain, H^+ and H^- are alternating along the [0001] direction, leading to an electrostatic attractive interaction that stabilizes the H chain structure, but the opposite is found along the $[1\bar{2}10]$ direction. Therefore, H chains are formed along the [0001] direction. We also calculated the adsorption coverage of hydrogen in 1 mbar of

https://doi.org/10.1021/jacs.3c08085
J. Am. Chem. Soc. 2023, 145, 22697−22707

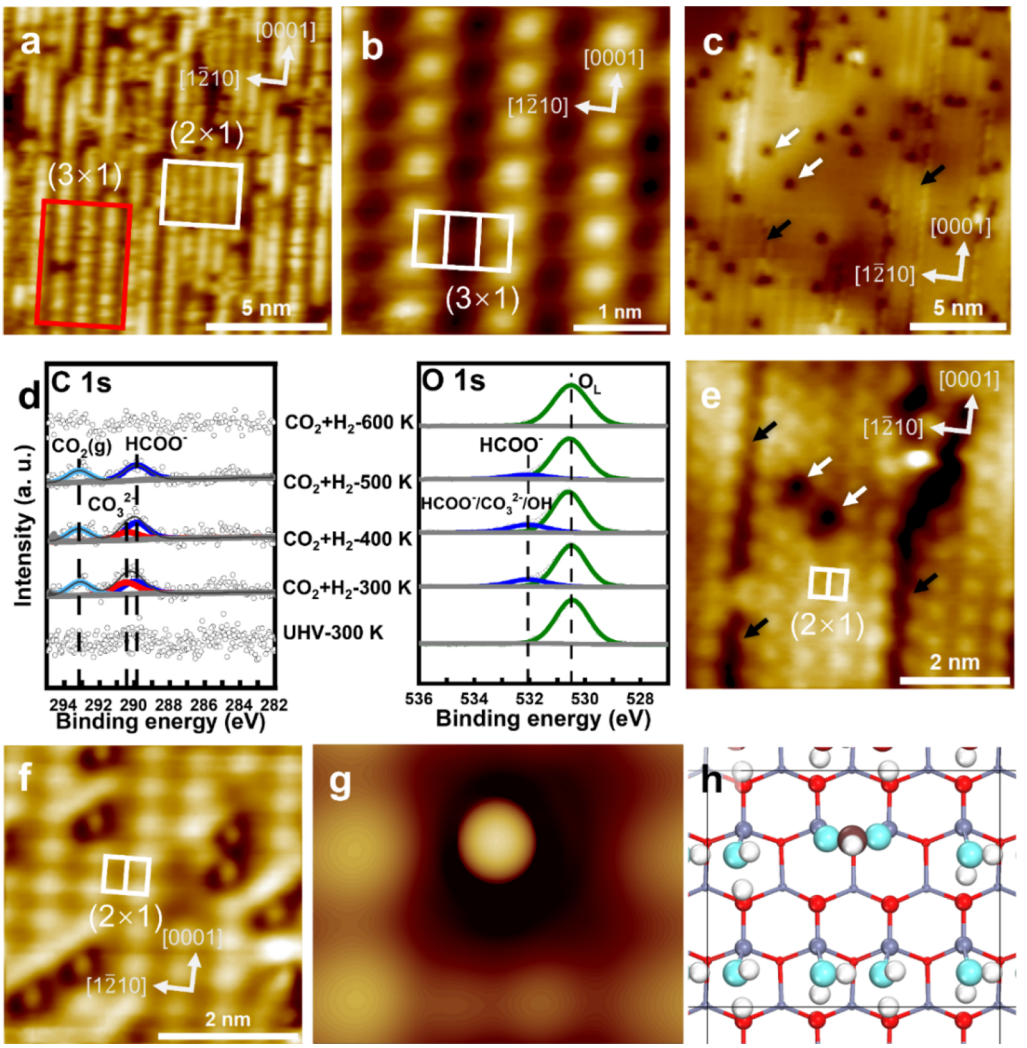

Figure 2. (a) STM image of ZnO(10$\bar{1}$0) during the exposure to a 1 mbar H_2/CO_2 (3:1) mixture gas at 300 K. The structure of the (3 × 1) domains is displayed in panel (b). (c) Large-scale STM image of surface adsorbates on ZnO(10$\bar{1}$0) after being annealed in 1 mbar H_2/CO_2 (3:1) mixture gas at 400 K. The formate species and adsorbed CO_2 are indicated by white and black arrows, respectively. (d) AP-XPS C 1s and O 1s of ZnO(10$\bar{1}$0) in 0.6 mbar H_2/CO_2 (3:1) mixture gas at different temperatures. Surface adsorbates on ZnO(10$\bar{1}$0) in panel (c) are resolved in panel (e). Upon evacuation to UHV, the formate species could be resolved more clearly in panel (f), along with the corresponding (g) simulated STM image and (h) structural model. Gray, red, green, brown, and white spheres represent Zn, lattice O, O in adsorbates, C atoms, and H atoms, respectively. Scanning parameters: (a) V_s = 2.5 V, I_t = 120 pA, (b) V_s = 2.7 V, I_t = 140 pA, (c) V_s = 2.5 V, I_t = 130 pA, (e) V_s = 2.1 V, I_t = 210 pA, and (f) V_s = 2.0 V, I_t = 190 pA.

H_2 at varying temperatures (Figure S6), which showed that hydrogen cannot saturate the ZnO surface due to the repulsion between neighboring H atoms along the [1$\bar{2}$10] direction. A trend of diminishing hydrogen surface coverage is observed with escalating temperatures. The differential charge density map (Figure S5d) shows that the electron density accumulates in the vicinity of H for the Zn−H bond, indicating the characteristics of an ionic bond, while the electron concentration between H and O suggests the covalent nature of the O−H bond. The distinct charge state and bond nature suggest that their reactivity could be drastically different for hydrogenation reactions.

3.2. Reaction between CO_2 and H_2 on ZnO(10$\bar{1}$0). Exposure of ZnO(10$\bar{1}$0) to CO_2 leads to the formation of surface carbonate species, which has been confirmed by near-edge X-ray absorption fine structure (NEXAFS)[58] and high-resolution electron energy loss spectroscopy (HREELS)[59] studies. DFT calculations[59] suggested that the optimal adsorbate structure for CO_2 manifests as a tridentate configuration, where the carbon atom forms a bond with a surface threefold coordinated O (O_{3c}) site, and both oxygen atoms in CO_2 interact with adjacent threefold coordinated Zn (Zn_{3c}) sites along the [0001] direction. Under UHV, CO_2 exposure on ZnO led to the formation of a densely packed (1 × 1) phase at below 90 K.[59] This structure undergoes a phase transformation to a (2 × 1) configuration at escalated temperatures, a process driven by the repulsive forces between carbonate species.[59] We have found the adsorbate structures of CO_2 would further transform to a uniform (3 × 1) configuration from UHV to ambient pressures.[60] We then studied CO_2 hydrogenation on ZnO(10$\bar{1}$0) in a 1 mbar mixture gas of H_2 and CO_2 (3:1) (Figure 2). At 300 K, exposure to this mixture resulted in the formation of adsorbate domains on the ZnO surface with (2 × 1) or (3 × 1) periodicity (Figure 2a). The structure of (3 × 1) domains (Figure 2b) is identical to the CO_2 adsorbate structure under pure CO_2 of ambient pressure, which has been determined to be a combination of 1/3 ML physisorbed CO_2 and 2/3 ML chemisorbed CO_2 in our study.[60] The adsorbate structure in the presence of H_2/CO_2 being different from the

https://doi.org/10.1021/jacs.3c08085
J. Am. Chem. Soc. 2023, 145, 22697−22707

uniform (3×1)-CO_2 structure in ambient CO_2 suggests that the structural changes in the CO_2 domains are due to the adsorption of hydride species, leading to the rearrangement of the CO_2 adsorbates and causing missing rows of CO_2. The adsorption energy of physisorbed CO_2 on ZnO$(10\bar{1}0)$ is −0.53 eV,[60] similar to the dissociative adsorption energy of H_2 of −0.48 eV. This means that physisorbed CO_2 cannot block surface sites for H_2 dissociation on ZnO, which also confirms that the dissociated hydrogen was able to coexist with CO_2 adsorbates on ZnO.

At elevated temperatures, AP-STM measurements showed the formation of new species, represented by dark spots on ZnO$(10\bar{1}0)$ in large-scale images (Figure 2c and Figure S7). The surface coverages of dark spots were 0.013, 0.035, and 0.070 ML when exposed to 1 mbar H_2/CO_2 (3:1) mixture gas at 400, 450, and 500 K, respectively (Figure S8a−c). Accordingly, AP-XPS measurements of CO_2 hydrogenation were carried out under 0.6 mbar of a H_2/CO_2 (3:1) mixture gas at elevated temperatures (Figure 2d). The emergence of the C 1s peak at 290.4 eV suggested the formation of carbonate species,[61,62] which would desorb completely from ZnO$(10\bar{1}0)$ at 500 K even in CO_2 (Figure S9). Figure 2d also shows a C 1s peak at 289.9 eV, which was stable at 500 K in H_2/CO_2 mixture gas and could be assigned as formate species.[61,63] Consistent with the increase in formate peak intensity in Figure 2d, STM results (Figure S8) also showed that the surface coverage of formate species increased from 300 to 500 K. Thus, the dark spots can be identified as formate species formed through the hydrogenation of CO_2 on ZnO.

During the exposure to the H_2/CO_2 mixture gas, adsorbate chains were adsorbed along the [0001] direction (Figure 2c,e and Figure S7). The dark linear adsorbates could be assigned as CO_2, which adsorbs more strongly than H_2 on ZnO. A similar chain structure has been observed for CO_2 adsorption on ZnO$(10\bar{1}0)$ under cryogenic conditions[64] or in the presence of CO_2 gas, although CO_2 chains are not stable in UHV (Figure S8). Note that CO_2 hydrogenation at elevated temperatures also led to the formation of water, which adsorbs strongly on ZnO$(10\bar{1}0)$ and forms a (2×1) adsorbate structure stable in UHV, which facilitated the desorption of CO_2 in the meantime (Figure 2f). The high-resolution STM image of formate species on the ZnO$(10\bar{1}0)$ surface in UHV (Figure 2f) shows the feature of bright dots with dark halos, similar to a previous UHV study of formic acid adsorption.[65] These formate species were located at the bridge site between neighboring Zn atoms, as corroborated from the DFT-simulated STM image and structural model (Figure 2g−h) of formate on ZnO$(10\bar{1}0)$ covered by water. The formation of water could be attributed to the reduction of ZnO steps by H_2, which could be evidenced by the curvy steps after the H_2 reaction (Figure S10). DFT calculations (Figure S11) confirmed the reduction of ZnO in 1×10^{-3} bar H_2 and showed that the step edges of ZnO$(10\bar{1}0)$ are easier to reduce than the terrace. However, the reduction reaction could stop in the presence of 10^{-10} bar H_2O. Although the etching of ZnO by H_2 is kinetically slow, it is sufficient to allow for surface hydroxylation. Figure 2h shows that H_2O adsorbates form a (2×1) structure on ZnO$(10\bar{1}0)$ at below 350 K, consistent with a previous study.[66] Note that the structural model of the (2×1) adsorbates that consists of alternative adsorption of hydroxyl and water (Figure 2h) was constructed based on a previous study.[66] Meanwhile, these $HCOO^-$ species formed via CO_2 hydrogenation exhibited room-temperature mobility, hopping randomly from one bridge site to another (Figure S12 and Movie S1).

DFT calculations indicate that formate species can easily be formed through the reaction of CO_2 with a hydride bonded to the surface Zn_{3c} site. Figure 3 shows that the energy barrier for

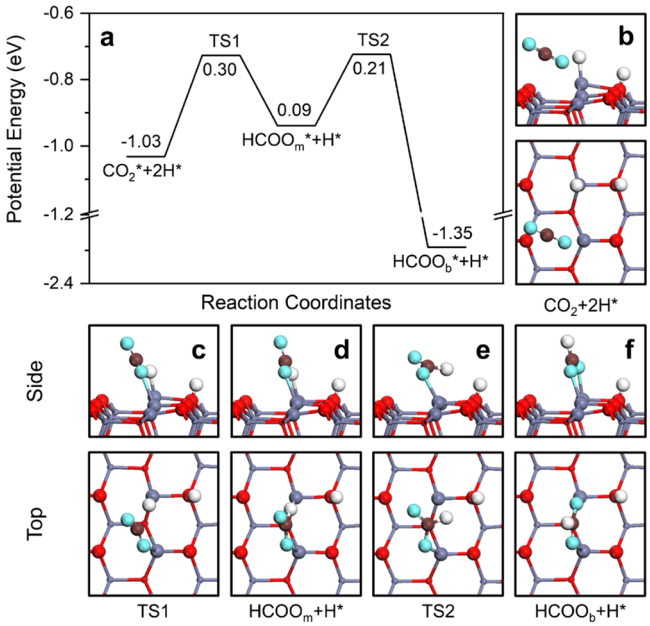

Figure 3. (a) Potential energy surface and (b−f) intermediate configurations and transition state configurations of CO_2 hydrogenation to HCOO* on the stoichiometric ZnO$(10\bar{1}0)$ surface. Gray, red, green, brown, and white spheres represent Zn, lattice O, O in adsorbates, C atoms, and H atoms, respectively.

binding CO_2 to the hydride species is as low as 0.30 eV, with a reaction energy of 0.09 eV. The formed formate species binds to the Zn_{3c} site in a monodendate configuration ($HCOO_m$*) via a Zn−O bond. It then undergoes structural relaxation by flipping over to form a bidentate coordination with two Zn_{3c} sites via two Zn−O bonds ($HCOO_b$*), which is exothermic by −1.35 eV with a low barrier of 0.21 eV. These calculations demonstrate that the formation of formate species is both thermodynamically and kinetically favorable from CO_2 and H_2, and the active sites for hydrogenation reactions are indeed surface Zn_{3c} sites bonded with hydride species. Combining AP-STM, AP-XPS, and DFT calculations, we confirmed formate species as key intermediates for CO_2 hydrogenation over ZnO and further hydrogenation of formate species as a rate-limiting step, as proposed from theoretical studies.[6,67]

3.3. Reaction between CO and H_2 on ZnO$(10\bar{1}0)$. When the mixture gas of H_2 and CO (3:1) was introduced to ZnO$(10\bar{1}0)$ at 300 K under ambient pressure, a coadsorption process was observed by AP-STM (Figure 4) since the adsorption energy of CO on ZnO$(10\bar{1}0)$ is only −0.58 eV,[60] similar to the dissociative adsorption energy of H_2 at −0.48 eV. In the presence of CO, the dissociative adsorption of H_2 was not inhibited, but the hydride chain growth turned more drastic and denser (Figures 1e and 4a). Instead of competitive adsorption, the surface coverage of hydride chains was found to increase to ∼0.06 ML, accompanying their increased diffusivity. Upon exposure, the hydride chain was first observed in STM (Figure 4a), while the appearance of the (2×1)-CO domain, same as the structure in pure CO,[60] became prominent with increasing

https://doi.org/10.1021/jacs.3c08085
J. Am. Chem. Soc. 2023, 145, 22697−22707

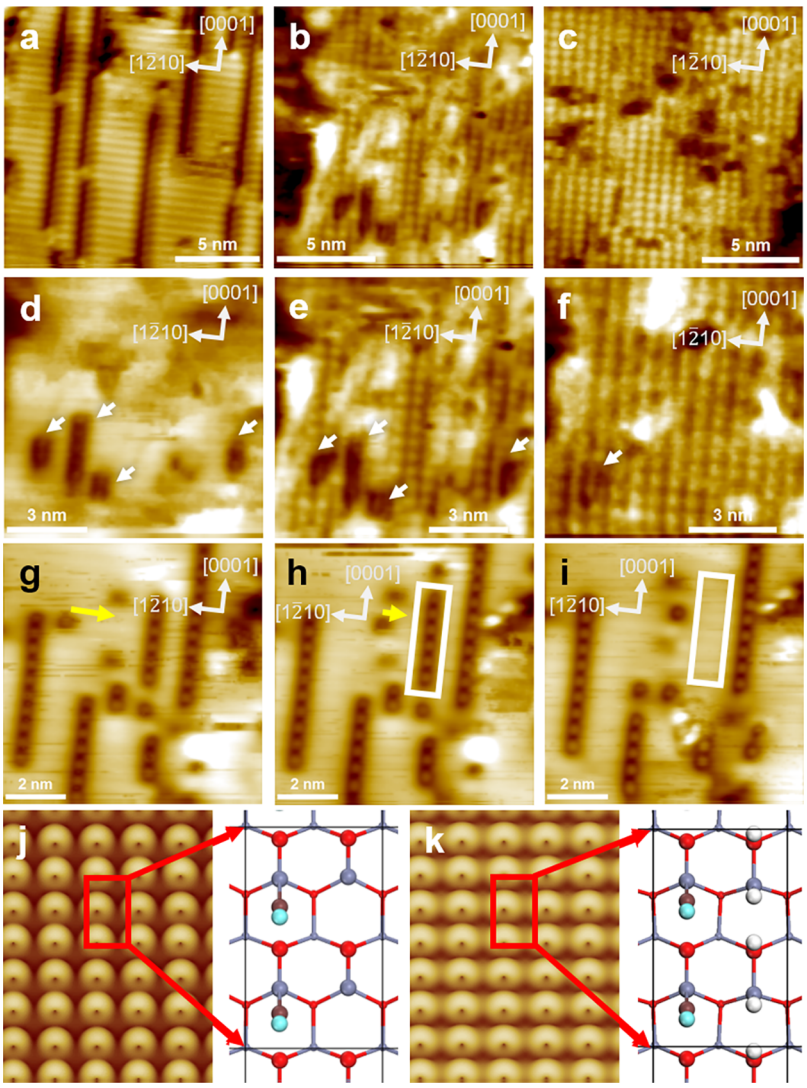

Figure 4. (a–c) STM images of ZnO(10$\bar{1}$0) during the exposure to H_2/CO mixture gas. (d–f) In situ STM images of ZnO(10$\bar{1}$0) during the exposure of 0.6 mbar H_2 + (d) 0.2 mbar CO, (e) 0.4 mbar CO, and (f) 0.6 mbar CO. The formation of hydride species is indicated by white arrows. (g–i) In situ STM images of hydride species on ZnO(10$\bar{1}$0) in 2 mbar H_2/CO (3:1) mixture gas at 300 K. White rectangles mark the disappearance of surface hydride species via the recombinative desorption of H_2. Yellow arrows indicate the diffusion of surface hydride species. (j, k) DFT-simulated STM images and corresponding structural models of (j) (2 × 1)-CO on ZnO(10$\bar{1}$0) and (k) coadsorption of CO and H_2. Gray, red, green, brown, and white spheres represent Zn, lattice O, O in adsorbates, C atoms, and H atoms, respectively. Scanning parameters: (a) V_s = 2.6 V, I_t = 100 pA, (b) V_s = 2.5 V, I_t = 140 pA, (c) V_s = 3.4 V, I_t = 140 pA, (d–f) V_s = 2.5 V, I_t = 140 pA, and (g–i) V_s = 2.4 V, I_t = 110 pA.

CO pressure (Figure 4b,c). The dynamic adsorption process could be better viewed by in situ STM measurements (Figure 4d–f), where surface hydride chains were in dynamic equilibrium with the mixture gas phase (Figure 4g–i), similar to the pure H_2 environment. As the CO pressure increases (Figure 4f), the (2 × 1)-CO domains covered the entire exposed surface of ZnO(10$\bar{1}$0), where surface hydride chains became difficult to detect by STM.

According to the DFT calculations, in a (2 × 1) supercell, the adsorption energy of CO on a clean ZnO(10$\bar{1}$0) surface is −0.58 eV, which changes to be −0.63 eV when it coadsorbs with a hydride–proton pair after H_2 dissociation. These results suggest a minor van der Waals attractive interaction between CO and its neighboring hydride species. In turn, CO also contributed to the enhanced stability of dissociated hydrogen molecules adsorbed on ZnO(10$\bar{1}$0), as evidenced by the notable rise in surface hydride coverage from ∼0.01 ML in pure hydrogen to ∼0.06 ML in the H_2/CO (3:1) gas mixture (Figures 1e and 4a). The DFT-based STM simulation shows almost no difference in simulated images between the (2 × 1)-CO structure on a clean surface (Figure 4j) and with coadsorbed H atoms from the heterolytic H_2 dissociation (Figure 4k). This implies that the surface hydride species can be stabilized in the CO environment but cannot be detected by STM (Figure 4c). The bright spots in the STM image are the 2π* antibonding states of CO molecules. The interaction between CO and the dissociated H_2 can be illustrated more specifically by vibration analysis. Theoretical calculation results indicate that the vibrational frequency of Zn–H bond stretching red-shifts from 1779 cm^{-1} without CO coadsorption to 1718 cm^{-1} coadsorbed with CO, while the frequency of H–O stretching blue-shifts from 3542 to 3578 cm^{-1} after CO coadsorption. These results are consistent with FTIR studies,[68] which also provide evidence that hydride can exist on the ZnO(10$\bar{1}$0) surface as a coadsorbed species at higher CO coverage.

https://doi.org/10.1021/jacs.3c08085
J. Am. Chem. Soc. 2023, 145, 22697–22707

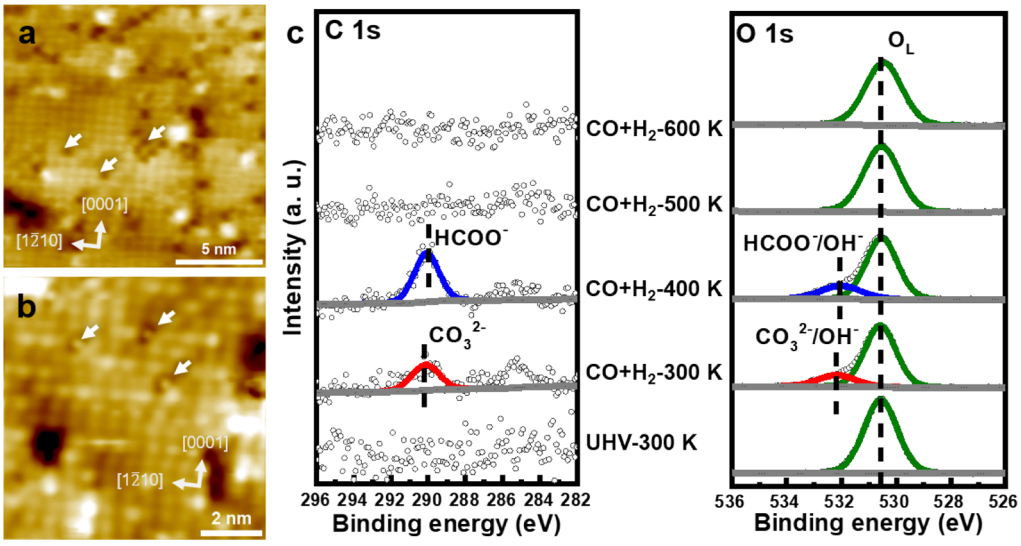

Figure 5. (a) STM image of surface adsorbates on ZnO(10$\bar{1}$0) after being annealed in a 1 mbar H_2/CO (3:1) mixture gas at 450 K. The formate species is indicated by white arrows and magnified in panel (b). (c) AP-XPS C 1s and O 1s of ZnO(10$\bar{1}$0) in the 0.6 mbar H_2/CO (3:1) mixture gas at different temperatures. Scanning parameters: (a) V_s = 4.0 V, I_t = 150 pA and (b) V_s = 2.8 V, I_t = 150 pA.

We then studied the CO hydrogenation reaction on ZnO(10$\bar{1}$0) by exposing the surface to the H_2/CO mixture gas at elevated temperatures (Figure 5). Similar to CO_2 hydrogenation, the reaction resulted in the formation of formate species (Figure 5a and Figure S13), which were observed as dark spots and mobile on the surface at even room temperature (Figure S14). The surface coverage of dark spots increased from 0.019 to 0.026 ML when the reaction temperature was raised from 400 to 450 K (Figure S13a,b) but decreased to 0.012 ML when the reaction was carried out at 500 K (Figure S13c). The surface coverage of formate species is much lower than that formed during CO_2 hydrogenation above 450 K. Formate species in the high-resolution STM image (Figure 5b) appeared as bright spots with dark halos, which further corroborated the above observation and assignment. The formation of $HCOO^-$ was also confirmed in AP-XPS by the appearance of a C 1s peak at 289.9 eV at 400 K (Figure 5c). Consistent with AP-STM results, the AP-XPS study also showed that formate species were almost undetectable during CO hydrogenation when the temperature was increased to 500 K (Figure 5c), compared to the significant formate peak observed during CO_2 hydrogenation at 500 K on ZnO(10$\bar{1}$0) (Figure 2d). In addition to formate species, a (2 × 1) adsorbate structure could also be observed after CO hydrogenation (Figure 5b), similar to the case of CO_2 hydrogenation, and was assigned to dissociated water species. Since hydroxyl groups were commonly observed surface adsorbates during hydrogenation reactions, their effect on hydrogenation, acting as an additional hydrogen species, warrants further scrutiny. A comprehensive study regarding this aspect is presented in the following section.

The formation of the $HCOO^-$ species involves both the oxidation of CO and the hydrogenation process, and it was believed that the lattice oxygen of ZnO would participate in the formation of $HCOO^-$. Interestingly, when the ZnO surface was annealed to 600 K to desorb all surface adsorbates, leaving only immobile defects on the surface (Figure S15), the surface coverage of these defects on the ZnO(10$\bar{1}$0) terrace is always less than 0.01 ML before and after CO hydrogenation at elevated temperatures, despite the formation of high-coverage formate species. This indicates that the additional oxygen in the $HCOO^-$ species formed through CO hydrogenation does not come from the terrace of ZnO(10$\bar{1}$0). Indeed, our study found that CO can easily react with O atoms at the ⟨0001⟩ step to form CO_2, which diffuses facilely to the ZnO(10$\bar{1}$0) terrace.[60]

DFT calculations were employed to identify the formation of formate species from CO and H_2. As shown in Figure 6, CO first binds with the hydride species to form HCO*, endothermic by 0.06 eV with an energy barrier of 0.61 eV. Afterward, the formed HCO* further reacts with the surface lattice O to form the formate of tridentate configuration ($HCOO_L$*), with an energy barrier of 1.06 eV and a reaction energy of −0.39 eV. In accordance with STM observation, the relatively high energy

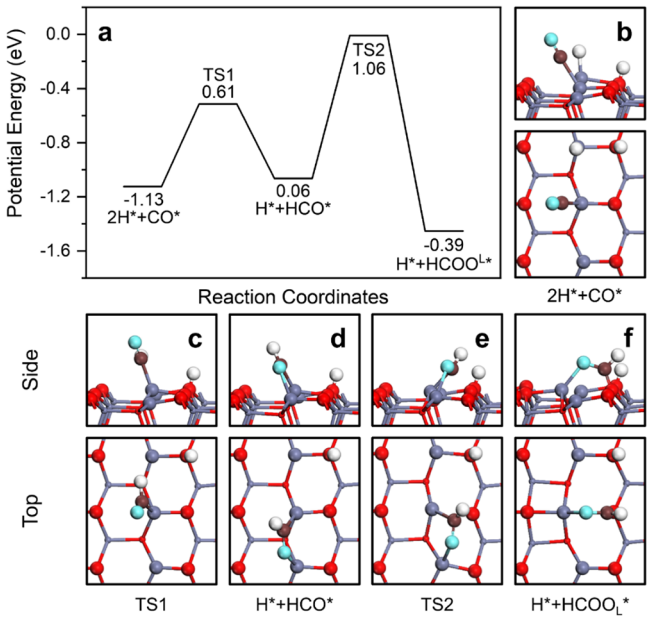

Figure 6. (a) Potential energy surface and (b–f) intermediate configurations and transition state configurations of CO hydrogenation to HCOO* on the stoichiometric ZnO(10$\bar{1}$0) surface. Gray, red, green, brown, and white spheres represent Zn, lattice O, O in adsorbates, C atoms, and H atoms, respectively.

https://doi.org/10.1021/jacs.3c08085
J. Am. Chem. Soc. 2023, 145, 22697−22707

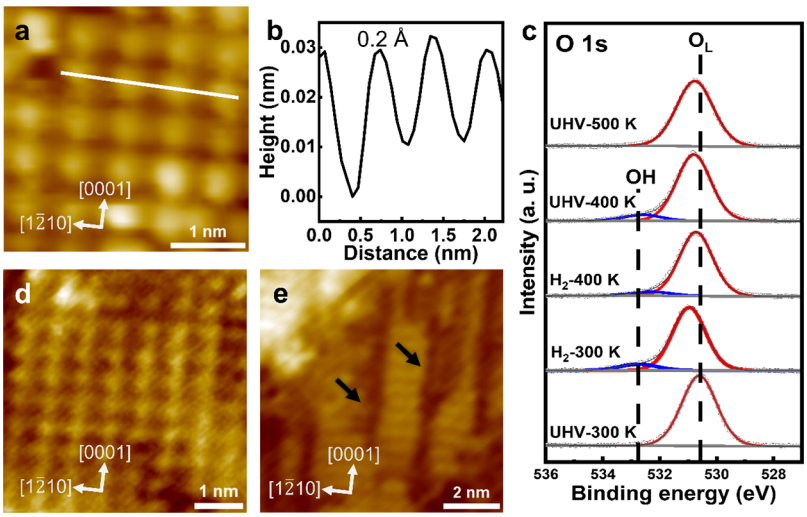

Figure 7. (a) STM image of the (2 × 1)-hydroxyl superstructure on ZnO(10$\bar{1}$0) after being annealed in 1 mbar of H_2 at 400 K. (b) Corresponding line profile of the solid line in panel (a). (c) AP-XPS O 1s spectra of ZnO(10$\bar{1}$0) in 1 mbar H_2 at different temperatures. STM images of the hydroxylated ZnO(10$\bar{1}$0) surface during the exposure to (d) 2.1 mbar CO at 300 K and (e) 1.1 mbar CO at 450 K. The black arrows indicate linear adsorbed CO_2. Scanning parameters: (a) V_s = 2.5 V, I_t = 100 pA, (d) V_s = 1.3 V, I_t = 200 pA, and (e) V_s = 2.4 V, I_t = 170 pA.

barrier of the formation of formate also suggests that the coupling reaction of the lattice O on terrace sites and the HCO* species is difficult to occur. In contrast, the HCO* species is favored to reversely dissociate into CO and hydride species due to its lower barrier (0.55 eV) than that of formate formation. Thus, CO can hardly be hydrogenated directly to form formate species. However, our study showed that CO oxidation at the ⟨0001⟩ step to form CO_2 is facile[60] and only needs to overcome a barrier of 0.46 eV (Figure S16). From the above section, the energy barriers for the hydrogenation of CO_2 by hydride species (0.30 eV) and the formation of bidentate $HCOO_b$* (0.21 eV) are both much lower than those for the transformation of HCO* to $HCOO_L$* (1.06 eV), as depicted in Figure 6. In this case, the mechanism of CO hydrogenation on ZnO(10$\bar{1}$0) is proposed as the following two-step mechanism: CO is first oxidized to CO_2 at the ⟨0001⟩ step of ZnO(10$\bar{1}$0). Then, the generated CO_2 will diffuse on the ZnO(10$\bar{1}$0) terrace and react with hydride species to form formate species.

3.4. Reaction of CO or CO_2 with Hydroxyl Groups on ZnO(10$\bar{1}$0). The heterolytic dissociation of H_2 on ZnO produced simultaneously hydroxyl and hydride species. To examine the effect of hydroxyl groups and rule out their role in the above hydrogenation experiments, we have prepared ZnO surfaces covered by hydroxyl groups exclusively and monitored their reactions with CO and CO_2 on ZnO(10$\bar{1}$0). The hydroxylated surface was prepared by annealing ZnO(10$\bar{1}$0) in 1 mbar of H_2 at 400 K, as monitored by AP-STM. The hydroxyls formed a (2 × 1) superstructure (Figure 7a) on ZnO(10$\bar{1}$0), which was also observed when water was directly introduced to the surface.[66] Upon surface hydroxylation, the hydroxyl groups displayed an apparent height of ~0.2 Å (Figure 7a,b) and remained stable even after H_2 evacuation, which could be used to differentiate the (2 × 1) structure of hydroxyls from those of CO or CO_2 on ZnO (Figure S17). AP-XPS measurements (Figure 7c) also confirmed the formation of hydroxyl groups in H_2 and their thermal stability in UHV with the O 1s peak at 532.5 eV. On hydroxylated ZnO surfaces, the formation of hydride chains in H_2 was not observed (Figure S10) due to the occupation of surface Zn sites by hydroxyl groups or water, preventing the dissociative adsorption of H_2 on the hydroxyl-covered surface.

When the hydroxylated ZnO(10$\bar{1}$0) surface was exposed to 2.1 mbar of CO at 300 K, there was no change in the (2 × 1) structure of the hydroxylated ZnO surface, as observed by AP-STM (Figure 7d and Figure S18a). CO adsorption on the hydroxylated ZnO(10$\bar{1}$0) surface is inhibited by the presence of hydroxyl groups. When the hydroxylated ZnO(10$\bar{1}$0) surface was heated to 450 K in the presence of CO, no formate species but adsorbate chains were observed along the [0001] direction on the surface (Figure 7e and Figure S18b). These adsorbate chains are assigned to CO_2 since the same linear structure and thermal stability were observed in CO_2 exposure on hydroxylated ZnO(10$\bar{1}$0) (Figure 2c and Figures S6 and S19). From AP-XPS, carbonate species formed on hydroxylated ZnO(10$\bar{1}$0) during the annealing in CO was not obvious from the O 1s spectra since the peak overlaps with the hydroxyl peak (Figure S20). Meanwhile, a trace amount of carbonate species was not sensitive for C 1s spectra from lab-based AP-XPS, which detected mainly the gas-phase CO peak at 291.8 eV (Figure S20). Note that carbonate species are less stable on hydroxylated ZnO(10$\bar{1}$0) and would decompose and desorb below 450 K.[69] These results suggest that hydroxyl groups on the surface do not facilitate the hydrogenation of CO but rather promote the oxidation of CO to CO_2 through the oxidation at step sites.

4. CONCLUSIONS

In summary, we have used AP-STM to directly visualize the heterolytic dissociation of H_2 on the ZnO(10$\bar{1}$0) surface and provided direct evidence that the formation of hydride species occurs on the surface terrace of ZnO and hydride is the active species for CO_x hydrogenation on ZnO. Combining AP-STM, AP-XPS, and DFT calculations, we show that H_2 dissociation does not need the assistance of surface defects on ZnO and hydrides are highly effective at hydrogenating CO or CO_2, while hydroxyl groups are not. The presence of CO or CO_2 did not block surface sites for the dissociation of H_2 on ZnO at 300 K. CO could even increase the stability of coadsorbed hydride species, facilitating their dissociative adsorption. Meanwhile, the transformation from hydrides to hydroxyls is facile on ZnO at

https://doi.org/10.1021/jacs.3c08085
J. Am. Chem. Soc. 2023, 145, 22697−22707

elevated temperatures, leading to a dominance of hydroxyl groups on the surface of ZnO. This in turn led to weakened adsorption of CO and CO_2 and hindered H_2 adsorption. As a result, hydrogenation of CO_x is unlikely to occur on a fully hydroxylated ZnO surface and must be carried out at above 450 K to facilitate the desorption of hydroxyls and enable hydrogenation to take place. Furthermore, CO_2 hydrogenation was found to be more favorable than CO hydrogenation on ZnO. We propose a two-step mechanism for CO hydrogenation, which involves the initial oxidation of CO to CO_2 at step sites on ZnO followed by a reaction with hydride to form formate. This proposition is supported by the substantial energy barriers for binding of CO with hydride and the absence of oxygen vacancies detected on the ZnO terrace following hydrogenation reaction. By shedding light on the CO_x hydrogenation reaction on ZnO, our study offers valuable molecular insights that deepen our understanding of syngas conversion and oxide catalysis in a broader context.

■ ASSOCIATED CONTENT

Supporting Information

The Supporting Information is available free of charge at https://pubs.acs.org/doi/10.1021/jacs.3c08085.

Movie S1: Diffusion of $HCOO^-$ species formed via CO_2 hydrogenation on ZnO($10\bar{1}0$) at 300 K (MP4)

Additional FTIR spectra, STM images, DFT calculation results, and AP-XPS spectra (Figures S1−S20) (PDF)

■ AUTHOR INFORMATION

Corresponding Authors

Wei-Xue Li − *Key Laboratory of Precision and Intelligent Chemistry, School of Chemistry and Materials Science, iChEM, University of Science and Technology of China, Hefei 230026, China; Hefei National Laboratory, University of Science and Technology of China, Hefei, Anhui 230088, China;* orcid.org/0000-0002-5043-3088; Email: wxli70@ustc.edu.cn

Fan Yang − *State Key Laboratory of Catalysis, Dalian Institute of Chemical Physics, Chinese Academy of Sciences, Dalian 116023, China; School of Physical Science and Technology, Center for Transformative Science, ShanghaiTech University, Shanghai 201210, China; Shanghai Key Laboratory of High-Resolution Electron Microscopy, ShanghaiTech University, Shanghai 201210, China;* orcid.org/0000-0002-1406-9717; Email: fyang@shanghaitech.edu.cn

Authors

Yunjian Ling − *State Key Laboratory of Catalysis, Dalian Institute of Chemical Physics, Chinese Academy of Sciences, Dalian 116023, China; School of Physical Science and Technology, Center for Transformative Science, ShanghaiTech University, Shanghai 201210, China; University of Chinese Academy of Sciences, Beijing 100039, China*

Jie Luo − *Hefei National Research Center for Physical Science at the Microscale, University of Science and Technology of China, Hefei 230026, China;* orcid.org/0000-0002-0932-8331

Yihua Ran − *School of Physical Science and Technology, Center for Transformative Science, ShanghaiTech University, Shanghai 201210, China*

Zhi Liu − *School of Physical Science and Technology, Center for Transformative Science, ShanghaiTech University, Shanghai 201210, China;* orcid.org/0000-0002-8973-6561

Complete contact information is available at: https://pubs.acs.org/10.1021/jacs.3c08085

Author Contributions

○Y.L. and J.L. contributed equally to this work.

Notes

The authors declare no competing financial interest.

■ ACKNOWLEDGMENTS

This work was financially supported by the National Natural Science Foundation of China (21972144, 22221003, 92045303, 91945302, M-0384, 21991152, and 22303089), Science and Technology Commission of Shanghai Municipality (20JC1416700 and 21DZ2260400), the Strategic Priority Research Program of the Chinese Academy of Sciences (XDB0450102), Innovation Program for Quantum Science and Technology (2021ZD0303302), K. C. Wong Education (GJTD-2020-15), and the China Postdoctoral Science Foundation (2023M733373). The authors thank the support from the Analytical Instrumentation Center, under contract number SPST-AIC10112914, at ShanghaiTech University and Supercomputing Center of University of Science and Technology of China. The authors thank Professor Xinhe Bao for the fruitful advice, discussions, and support of the project and thank Professors Christof Wöll and Xiang Shao for fruitful discussions.

■ REFERENCES

(1) Subramani, V.; Gangwal, S. K. A review of recent literature to search for an efficient catalytic process for the conversion of syngas to ethanol. *Energy Fuels* **2008**, *22* (2), 814−839.

(2) Martin, O.; Martin, A. J.; Mondelli, C.; Mitchell, S.; Segawa, T. F.; Hauert, R.; Drouilly, C.; Curulla-Ferre, D.; Perez-Ramirez, J. Indium Oxide as a Superior Catalyst for Methanol Synthesis by CO_2 Hydrogenation. *Angew. Chem., Int. Ed.* **2016**, *55* (21), 6261−6265.

(3) Pan, X.; Jiao, F.; Miao, D.; Bao, X. Oxide-Zeolite-Based Composite Catalyst Concept That Enables syngas Chemistry beyond Fischer−Tropsch Synthesis. *Chem. Rev.* **2021**, *121* (11), 6588−6609.

(4) Jiao, F.; Li, J.; Pan, X.; Xiao, J.; Li, H.; Ma, H.; Wei, M.; Pan, Y.; Zhou, Z.; Li, M.; et al. Selective conversion of syngas to light olefins. *Science* **2016**, *351* (6277), 1065−1068.

(5) Li, N.; Jiao, F.; Pan, X. L.; Ding, Y.; Feng, J. Y.; Bao, X. H. Size Effects of ZnO Nanoparticles in Bifunctional Catalysts for Selective syngas Conversion. *ACS Catal.* **2019**, *9* (2), 960−966.

(6) Kattel, S.; Ramirez, P. J.; Chen, J. G.; Rodriguez, J. A.; Liu, P. Active sites for CO_2 hydrogenation to methanol on Cu/ZnO catalysts. *Science* **2017**, *355* (6331), 1296−1299.

(7) Palomino, R. M.; Ramirez, P. J.; Liu, Z. Y.; Hamlyn, R.; Waluyo, I.; Mahapatra, M.; Orozco, I.; Hunt, A.; Simonovis, J. P.; Senanayake, S. D. Hydrogenation of CO_2 on ZnO/Cu(100) and ZnO/Cu(111) Catalysts: Role of Copper Structure and Metal-Oxide Interface in Methanol Synthesis. *J. Phys. Chem. B* **2018**, *122* (2), 794−800.

(8) Jiao, F.; Bai, B.; Li, G.; Pan, X. L.; Ye, Y. H.; Qu, S. C.; Xu, C. Q.; Xiao, J. P.; Jia, Z. H.; Liu, W.; et al. Disentangling the activity-selectivity trade-off in catalytic conversion of syngas to light olefins. *Science* **2023**, *380* (6646), 727−730.

(9) Behrens, M.; Studt, F.; Kasatkin, I.; Kuhl, S.; Havecker, M.; Abild-Pedersen, F.; Zander, S.; Girgsdies, F.; Kurr, P.; Kniep, B. L.; et al. The active site of methanol synthesis over $Cu/ZnO/Al_2O_3$ industrial catalysts. *Science* **2012**, *336* (6083), 893−897.

(10) Fujita, S.; Usui, M.; Takezawa, N. MECHANISM OF THE REVERSE WATER GAS SHIFT REACTION OVER CU/ZNO CATALYST. *J. Catal.* **1992**, *134* (1), 220−225.

(11) Mahapatra, M.; Gutiérrez, R. A.; Kang, J.; Rui, N.; Hamlyn, R.; Liu, Z.; Orozco, I.; Ramírez, P. J.; Senanayake, S. D.; Rodriguez, J. A. The behavior of inverse oxide/metal catalysts: CO oxidation and water-

gas shift reactions over ZnO/Cu(111) surfaces. *Surf. Sci.* **2019**, *681*, 116−121.
(12) Mehar, V.; Huang, E.; Shi, R.; Rui, N.; Rosales, R.; Waluyo, I.; Hunt, A.; Liu, P.; Rodriguez, J. A. Microscopic Investigation of H2 Reduced CuOx/Cu(111) and ZnO/CuOx/Cu(111) Inverse Catalysts: STM, AP-XPS, and DFT Studies. *ACS Catal.* **2023**, *13*, 9857−9870.
(13) Kurtz, M.; Strunk, J.; Hinrichsen, O.; Muhler, M.; Fink, K.; Meyer, B.; Woll, C. Active sites on oxide surfaces: ZnO-catalyzed synthesis of methanol from CO and H_2. *Angew. Chem., Int. Ed. Engl.* **2005**, *44* (18), 2790−2794.
(14) Zhang, L.; Zhang, X.; Qian, K.; Li, Z.; Cheng, Y.; Daemen, L.; Wu, Z.; Huang, W. Activation and surface reactions of CO and H-2 on ZnO powders and nanoplates under CO hydrogenation reaction conditions. *J. Energy Chem.* **2020**, *50*, 351−357.
(15) Wilmer, H.; Kurtz, M.; Klementiev, K. V.; Tkachenko, O. P.; Grunert, W.; Hinrichsen, O.; Birkner, A.; Rabe, S.; Merz, K.; Driess, M.; et al. Methanol synthesis over ZnO: A structure-sensitive reaction? *Phys. Chem. Chem. Phys.* **2003**, *5* (20), 4736−4742.
(16) Dent, A. L.; Kokes, R. J. Hydrogenation of ethylene by zinc oxide. II. Mechanism and active sites. *J. Phys. Chem.* **1969**, *73* (11), 3781−3790.
(17) Lai, Z.; Sun, N.; Jin, J.; Chen, J.; Wang, H.; Hu, P. Resolving the Intricate Mechanism and Selectivity of syngas Conversion on Reduced $ZnCr_2O_x$: A Quantitative Study from DFT and Microkinetic Simulations. *ACS Catal.* **2021**, *11* (21), 12977−12988.
(18) Liu, X.; Luo, J.; Wang, H.; Huang, L.; Wang, S.; Li, S.; Sun, Z.; Sun, F.; Jiang, Z.; Wei, S.; et al. In Situ Spectroscopic Characterization and Theoretical Calculations Identify Partially Reduced ZnO_{1-x}/Cu Interfaces for Methanol Synthesis from CO_2. *Angew. Chem., Int. Ed* **2022**, *61* (23), No. e202202330.
(19) Menetrey, M.; Markovits, A.; Minot, C. Reactivity of a reduced metal oxide surface: hydrogen, water and carbon monoxide adsorption on oxygen defective rutile TiO_2(110). *Surf. Sci.* **2003**, *524* (1−3), 49−62.
(20) Li, Z.; Werner, K.; Qian, K.; You, R.; Płucienik, A.; Jia, A.; Wu, L.; Zhang, L.; Pan, H.; Kuhlenbeck, H.; et al. Oxidation of Reduced Ceria by Incorporation of Hydrogen. *Angew. Chem., Int. Ed.* **2019**, *58* (41), 14686−14693.
(21) Gribov, E. N.; Bertarione, S.; Scarano, D.; Lamberti, C.; Spoto, G.; Zecchina, A. Vibrational and thermodynamic properties of H-2 adsorbed on MgO in the 300−20 K interval. *J. Phys. Chem. B* **2004**, *108* (41), 16174−16186.
(22) Joubert, J.; Salameh, A.; Krakoviack, V.; Delbecq, F.; Sautet, P.; Coperet, C.; Basset, J. M. heterolytic splitting of H_2 and CH_4 on gamma-alumina as a structural probe for defect sites. *J. Phys. Chem. B* **2006**, *110* (47), 23944−23950.
(23) Meriaudeau, P.; Primet, M. FTIR study of hydrogen adsorption on α-Ga_2O_3. *J. Mol. Catal.* **1990**, *61* (2), 227−234.
(24) Busca, G. Fourier transform-infrared spectroscopic study of the adsorption of hydrogen on chromia and on some metal chromites. *J. Catal.* **1989**, *120* (2), 303−313.
(25) Rossmuller, G.; Kleinschmidt, V.; Kossmann, J.; Hattig, C. A Density Functional Study of the Methanol Synthesis at an Oxygen Vacancy on the Polar ZnO(000$\bar{1}$) Surface. *J. Phys. Chem. C* **2009**, *113* (4), 1418−1425.
(26) Boccuzzi, F.; Borello, E.; Zecchina, A.; Bossi, A.; Camia, M. Infrared Study of Zno Surface Properties 0.1. Hydrogen and Deuterium Chemisorption at Room-Temperature. *J. Catal.* **1978**, *51* (2), 150−159.
(27) Wu, Z. L.; Cheng, Y. Q.; Tao, F.; Daemen, L.; Foo, G. S.; Nguyen, L.; Zhang, X. Y.; Beste, A.; Ramirez-Cuesta, A. J. Direct Neutron Spectroscopy Observation of Cerium Hydride Species on a Cerium Oxide Catalyst. *J. Am. Chem. Soc.* **2017**, *139* (28), 9721−9727.
(28) Copéret, C.; Estes, D. P.; Larmier, K.; Searles, K. Isolated Surface Hydrides: Formation, Structure, and Reactivity. *Chem. Rev.* **2016**, *116* (15), 8463−8505.
(29) Zhong, J.-Q.; Han, Z.-K.; Werner, K.; Li, X.-Y.; Gao, Y.; Shaikhutdinov, S.; Freund, H.-J. Water-Assisted Homolytic Dissociation of Propyne on a Reduced Ceria Surface. *Angew. Chem., Int. Ed.* **2020**, *59* (15), 6150−6154.
(30) Scarano, D.; Spoto, G.; Bordiga, S.; Zecchina, A.; Lamberti, C. LATERAL INTERACTIONS IN CO ADLAYERS ON PRISMATIC ZNO FACES - A FTIR AND HRTEM STUDY. *Surf. Sci.* **1992**, *276* (1−3), 281−298.
(31) Li, N.; Jiao, F.; Pan, X.; Ding, Y.; Feng, J.; Bao, X. Size Effects of ZnO Nanoparticles in Bifunctional Catalysts for Selective syngas Conversion. *ACS Catal.* **2019**, *9* (2), 960−966.
(32) Cremer, P. S.; Su, X.; Shen, Y. R.; Somorjai, G. A. Ethylene Hydrogenation on Pt(111) Monitored in Situ at High Pressures Using Sum Frequency Generation. *J. Am. Chem. Soc.* **1996**, *118* (12), 2942−2949.
(33) Somorjai, G. A.; Li, Y. *Introduction to surface chemistry and catalysis*. 2nd ed.; John Wiley & Sons: New York, 2010; pp 559−762.
(34) Chen, H.; Lin, L.; Li, Y.; Wang, R.; Gong, Z.; Cui, Y.; Li, Y.; Liu, Y.; Zhao, X.; Huang, W.; et al. CO and H-2 Activation over g-ZnO Layers and w-ZnO(0001). *ACS Catal.* **2019**, *9* (2), 1373−1382.
(35) Liu, Q.; Han, Y.; Cao, Y.; Li, X.; Huang, W.; Yu, Y.; Yang, F.; Bao, X.; Li, Y.; Liu, Z. In-situ APXPS and STM Study of the Activation of H-2 on ZnO(10$\bar{1}$0) Surface. *Acta Phys., Chim. Sin.* **2018**, *34* (12), 1366−1372.
(36) Cao, Y.; Luo, J.; Huang, W.; Ling, Y.; Zhu, J.; Li, W. X.; Yang, F.; Bao, X. Probing surface defects of ZnO using formaldehyde. *J. Chem. Phys.* **2020**, *152* (7), 8.
(37) Kresse, G.; Furthmüller, J. Efficient iterative schemes forab initiototal-energy calculations using a plane-wave basis set. *Phys. Rev. B* **1996**, *54* (16), 11169−11186.
(38) Blöchl, P. E. Projector augmented-wave method. *Phys. Rev. B* **1994**, *50* (24), 17953−17979.
(39) Kresse, G.; Joubert, D. From ultrasoft pseudopotentials to the projector augmented-wave method. *Phys. Rev. B* **1999**, *59* (3), 1758−1775.
(40) Klimeš, J.; Bowler, D. R.; Michaelides, A. Van der Waals density functionals applied to solids. *Phys. Rev. B* **2011**, *83* (19), 195131.
(41) Perdew, J. P.; Burke, K.; Ernzerhof, M. Generalized Gradient Approximation Made Simple. *Phys. Rev. Lett.* **1996**, *77* (18), 3865−3868.
(42) Gu, X.-K.; Qiao, B.; Huang, C.-Q.; Ding, W.-C.; Sun, K.; Zhan, E.; Zhang, T.; Liu, J.; Li, W.-X. Supported Single Pt1/Au1 Atoms for Methanol Steam Reforming. *ACS Catal.* **2014**, *4* (11), 3886−3890.
(43) Gu, X.-K.; Huang, C.-Q.; Li, W.-X. First-principles study of single transition metal atoms on ZnO for the water gas shift reaction. *Catalysis Science & Technology* **2017**, *7* (19), 4294−4301.
(44) Escudero, R.; Escamilla, R. Ferromagnetic behavior of high-purity ZnO nanoparticles. *Solid State Commun.* **2011**, *151* (2), 97−101.
(45) Abrahams, S. C.; Bernstein, J. L. Remeasurement of the structure of hexagonal ZnO. *Acta Crystallographica Section B* **1969**, *25* (7), 1233−1236.
(46) Henkelman, G.; Jónsson, H. Improved tangent estimate in the nudged elastic band method for finding minimum energy paths and saddle points. *J. Chem. Phys.* **2000**, *113* (22), 9978−9985.
(47) Henkelman, G.; Uberuaga, B. P.; Jónsson, H. A climbing image nudged elastic band method for finding saddle points and minimum energy paths. *J. Chem. Phys.* **2000**, *113* (22), 9901−9904.
(48) Tersoff, J.; Hamann, D. R. Theory and Application for the Scanning Tunneling Microscope. *Phys. Rev. Lett.* **1983**, *50* (25), 1998−2001.
(49) Tersoff, J.; Hamann, D. R. THEORY OF THE SCANNING TUNNELING MICROSCOPE. *Phys. Rev. B* **1985**, *31* (2), 805−813.
(50) Wang, B.; Ma, X.; Caffio, M.; Schaub, R.; Li, W.-X. Size-Selective Carbon Nanoclusters as Precursors to the Growth of Epitaxial Graphene. *Nano Lett.* **2011**, *11* (2), 424−430.
(51) Hofer, W. A. Challenges and errors: interpreting high resolution images in scanning tunneling microscopy. *Prog. Surf. Sci.* **2003**, *71* (5), 147−183.
(52) Wang, H.; Zhao, X.; Huang, C.; Jin, X.; Wei, D.; Dai, D.; Ma, Z.; Li, W.-X.; Yang, X. Adsorption Features of Formaldehyde on

TiO_2(110) Surface Probed by High-Resolution Scanning Tunnelling Microscopy. *J. Phys. Chem. Lett.* **2019**, *10* (12), 3352−3358.
(53) Wei, D.; Jin, X.; Huang, C.; Dai, D.; Ma, Z.; Li, W.-X.; Yang, X. Direct Imaging Single Methanol Molecule Photocatalysis on Titania. *J. Phys. Chem. C* **2015**, *119* (31), 17748−17754.
(54) Shi, H.; Yuan, H.; Li, Z.; Wang, W.; Li, Z.; Shao, X. Low-Temperature heterolytic Adsorption of H2 on ZnO($10\bar{1}0$) Surface. *J. Phys. Chem. C* **2019**, *123* (21), 13283−13287.
(55) Wintterlin, J.; Schuster, R.; Ertl, G. Existence of a "hot" atom mechanism for the dissociation of O-2 on Pt(111). *Phys. Rev. Lett.* **1996**, *77* (1), 123−126.
(56) Luo, J.; Liu, J.-X.; Li, W.-X. H_2 Activation on Pristine and Substitutional ZnO($10\bar{1}0$) and Cr_2O_3(001) Surfaces by Density Functional Theory Calculations. *J. Phys. Chem. C* **2022**, *126* (21), 9059−9068.
(57) Mun, B. S.; Liu, Z.; Motin, M. A.; Roy, P. C.; Kim, C. M. In situ observation of H_2 dissociation on the ZnO (0001) surface under high pressure of hydrogen using ambient-pressure XPS. *Int. J. Hydrogen Energy* **2018**, *43* (18), 8655−8661.
(58) Davis, R.; Walsh, J. F.; Muryn, C. A.; Thornton, G.; Dhanak, V. R.; Prince, K. C. THE ORIENTATION OF FORMATE AND CARBONATE ON ZNO $10\bar{1}0$. *Surf. Sci.* **1993**, *298* (1), L196−L202.
(59) Wang, Y.; Kovacik, R.; Meyer, B.; Kotsis, K.; Stodt, D.; Staemmler, V.; Qiu, H.; Traeger, F.; Langenberg, D.; Muhler, M.; et al. CO_2 activation by ZnO through the formation of an unusual tridentate surface carbonate. *Angew. Chem., Int. Ed. Engl.* **2007**, *46* (29), 5624−5627.
(60) Ling, Y.; Luo, J.; Ran, Y.; Cao, Y.; Huang, W.; Cai, J.; Liu, Z.; Li, W.; Yang, F.; Bao, X. Dynamic chemical processes on ZnO surfaces tuned by physisorption under ambient conditions. *J. Energy Chem.* **2022**, *72*, 258−264.
(61) Au, C. T.; Hirsch, W.; Hirschwald, W. ADSORPTION AND INTERACTION OF CARBON-DIOXIDE, FORMIC-ACID AND HYDROGEN CARBON-DIOXIDE MIXTURES ON (1010) ZINC-OXIDE SURFACES STUDIED BY PHOTOELECTRON-SPECTROSCOPY (XPS AND UPS). *Surf. Sci.* **1988**, *199* (3), 507−517.
(62) Kotsis, K.; Stodt, D.; Staemmler, V.; Kovacik, R.; Meyer, B.; Traeger, F.; Langenberg, D.; Strunskus, T.; Kunat, M.; Woll, C. CO_2 adlayers on the mixed terminated ZnO(10−10) surface studied by he atom scattering, photoelectron spectroscopy and ab initio electronic structure calculations. *Z. Phys. Chemie-Int. J. Res. Phys. Chem. Chem. Phys.* **2008**, *222* (5−6), 891−915.
(63) Senanayake, S. D.; Ramirez, P. J.; Waluyo, I.; Kundu, S.; Mudiyanselage, K.; Liu, Z. Y.; Liu, Z.; Axnanda, S.; Stacchiola, D. J.; Evans, J.; et al. Hydrogenation of CO_2 to Methanol on CeO_x/Cu(111) and ZnO/Cu(111) Catalysts: Role of the Metal-Oxide Interface and Importance of Ce^{3+} Sites. *J. Phys. Chem. C* **2016**, *120* (3), 1778−1784.
(64) Shi, H.; Ruan, S. Q.; Liu, H. H.; Wang, L.; Wang, W. Y.; Ren, X. G.; Wang, B.; Wu, K.; Shao, X. Directional Growth of One-Dimensional CO_2 Chains on ZnO($10\bar{1}0$). *J. Phys. Chem. C* **2016**, *120* (41), 23669−23674.
(65) Li, Z.; Yuan, H.; Sun, Y.; Zhang, J.; Li, Z.; Shao, X. Dissociative adsorption and linear organization of formic acid on ZnO (10−10) surface. *J. Catal.* **2020**, *390*, 109−116.
(66) Meyer, B.; Marx, D.; Dulub, O.; Diebold, U.; Kunat, M.; Langenberg, D.; Woll, C. Partial dissociation of water leads to stable superstructures on the surface of zinc oxide. *Angew. Chem., Int. Ed.* **2004**, *43* (48), 6642−6645.
(67) Kattel, S.; Liu, P.; Chen, J. G. Tuning Selectivity of CO_2 Hydrogenation Reactions at the Metal/Oxide Interface. *J. Am. Chem. Soc.* **2017**, *139* (29), 9739−9754.
(68) Griffin, G. L.; Yates, J. T. coadsorption studies of CO and H_2 on ZnO. *J. Chem. Phys.* **1982**, *77* (7), 3751−3758.
(69) Noei, H.; Woll, C.; Mahler, M.; Wang, Y. M. Activation of Carbon Dioxide on ZnO Nanoparticles Studied by Vibrational Spectroscopy. *J. Phys. Chem. C* **2011**, *115* (4), 908−914.

https://doi.org/10.1021/jacs.3c08085
J. Am. Chem. Soc. 2023, 145, 22697−22707